CTU Journal of Innovation and Sustainable Development
ISSN 2588-1418 | e-ISSN 2815-6412

DOI:10.22144/ctujoisd.2025.016

Synthesis of Fe_3O_4@Zeolite NaA from rice husk ash for efficient methylene blue adsorption

Luong Huynh Vu Thanh[1,2*], Huynh Quoc Bao[1,3], Nguyen Duc Nhan[1,3], Nguyen Viet Nhan Hoa[2], Thieu Quang Quoc Viet[2], and Le Thanh Phu[1,3]

[1]*Applied Chemical Engineering Lab, College of Engineering, Can Tho University, Viet Nam*

[2]*Faculty of Chemical Engineering, College of Engineering, Can Tho University, Viet Nam*

[3]*Course 45 of Chemical Engineering Program, Faculty of Chemical Engineering, Can Tho University, Viet Nam*

**Corresponding author (lhvthanh@ctu.edu.vn)*

Article info.

Received 1 Feb 2024
Revised 19 Feb 2024
Accepted 19 Aug 2024

Keywords

Adsorption, Fe_3O_4@zeolite NaA, Ferromagnetic particles, Methylene blue, Rice husk ash

ABSTRACT

This study synthesized Fe_3O_4@zeolite NaA with SiO_2 from rice husk ash and evaluated its adsorption of methylene blue from water. As-synthesized adsorbent was characterized by advanced analytical methods. The results showed that the adsorbent was in the size of 0.981±0.235 µm with a cubic and spherical shape and its specific surface area, pore diameter, and pore volume of 82.41 m^2/g, 1.019 nm, and 0.224 cm^3/g, respectively. The Fe_3O_4@zeolite NaA magnetization was 17.65 emu/g, and its point of zero charge was at 7.48. The adsorption achieved the highest efficiency of 86.5% at room temperature, pH 9 within 25 min with an initial concentration of 20 mg/L. This adsorption was a physical interaction and fitted to pseudo-second-order kinetics and Freundlich isotherm. Fe_3O_4@zeolite NaA was magnetically separated from the solution using a magnet and could be reused for two to three cycles. These findings suggested that Fe_3O_4@zeolite NaA can be a potential adsorbent for dye removal in industry.

1. INTRODUCTION

Water is one of the most important resources needed by all living beings. However, due to the rapid development in production of the textile and plastic industries, methylene blue (MB) has become a by-product of industrial production and is considered an untreated pollutant in wastewater (Chandrakant et al., 2016). Methylene blue (3,7-bis (dimethyla-mino)-phenothiazin-5- iumchloride) is a cationic thiazine dye commonly used for biological dyeing and dyeing of paper, hair, cotton, and wool. The accumulation of MB, a persistent organic pollutant, in wastewater can destroy aquatic life and humans (Oladoye, 2022). Therefore, it is necessary to find an efficient method to remove MB from wastewater before discharging into the environment. Amongst common techniques such as advanced oxidation, chemical oxidation, filtration, coagulation-flocculation, aerobic, anaerobic, and anoxic, adsorption stands up as a potential candidate due to its low cost, high efficiency and easy operation (Chandrakant et al., 2016).

To treat organic pollution using adsorption, many adsorbents have been employed, which are various from activated carbon, polymeric resins, and biochar to fly ash, bentonite clay, or zeolite (Galán et al., 2013; Chandrakant et al., 2016). Among these adsorbents, zeolite has been commonly applied to decolorize textile wastewater (EL-Mekkawi et al., 2016). However, the zeolite adsorption process has

difficulty in separating the adsorbed substance from the process (Velarde et al., 2023). The methods commonly used to separate the adsorbent from the solution are sedimentation and filtration. Nevertheless, it takes more time, and the efficiency is also low. To overcome the above disadvantages, a few studies have combined zeolite adsorbents with nano Fe_3O_4 to separate the adsorbent properties from the solution more easily, such as the study of attaching Fe_3O_4 to surface of zeolite NaA to form nanocomposite adsorbent for MB removal (Tran et al., 2021), adsorption of Cr(IV) ion using zeolite NaA coated Fe_3O_4 composite (Mai et al., 2021), the effect of zeolite NaA supplemented with Fe_3O_4 to remove ammonium ions (Liu et al., 2013a), or research on using magnetic nano-coated with zeolite NaA to remove Pb(II) ions and Cu(II) in water (Liu et al., 2013b). The above methods highlighted the important advantage of magnetically separating adsorbents from the solution using ferromagnetic nanoparticles. However, a new drawback appeared when a core of zeolite NaA was coated by a shell of Fe_3O_4 to form a NaA/Fe_3O_4 structure. This caused a reduction in adsorption surface area, thereby reducing the adsorption efficiency. Therefore, to further overcome the above drawback, this study proposes a method to synthesize Fe_3O_4@zeolite NaA with a core of iron nano form and a shell of zeolite NaA, without affecting the adsorption surface of zeolite NaA but still enough magnetism to separate the adsorbent from the aqueous solution.

To synthesize zeolite NaA, a good deal of silica resources has been utilized, namely sodium aluminosilicate solutions, metakaolin, rice husk ash, coal fly ash, silatrane or tetraethylorthosilicate (Khaleque et al., 2020). Rice husk is an agricultural by-product, which is abundant in rice production areas such as the Mekong Delta, Viet Nam, and has been used as a fuel in small factories. However, the disadvantage of this burning process is the accumulation of rice husk ash (RHA), which contains up to 80-90% crystalline silica (Zhang et al., 2013). This waste has been used as a natural silica source for the synthesis of zeolite NaA without using expensive synthetic precursors such as sodium aluminosilicate solutions, silatrane, or tetraethylorthosilicate (Yusof et al., 2010).

In this study, RHA was applied as an available SiO_2 source to synthesize zeolite NaA. For the first time, the material Fe_3O_4@zeolite NaA with a core of iron nano form and a shell of zeolite NaA was prepared and applied to remove MB in water. The influence of some conditions in the adsorption process, including pH solution, initial concentration of MB, adsorbent mass, and contact time, were studied. Adsorption isotherm and kinetic studies on MB separation were also investigated.

2. MATERIALS AND METHOD

2.1. Chemicals and materials

Ferric chloride ($FeCl_3.6H_2O$, 99%), sodium hydroxide (NaOH, 96%), hydrochloric acid (HCl, 38%), ammonia solution (NH_3, 25%) and Methylene Blue organic dye (MB, 99.5%) from Xilong Chem (China), sodium borohydride ($NaBH_4$, 99.5%) and (Poly)vinylpyrrolidone (PVP10) from Sigma-Aldrich (Germany) sodium aluminate ($NaAlO_2$, 99%) from Tianqin scientific Co. (China) were main chemicals used in this study. In addition, silica source (SiO_2) was recovered from rice husk ash. Distilled water was from the Applied Chemical Engineering Laboratory at Can Tho University.

2.2. Synthesis and characterization of Fe_3O_4@zeolite NaA

2.2.1. Synthesis of Fe_3O_4@SiO_2

To recover SiO_2 from rice husk ash (RHA), RHA was first collected from Duc An brick kiln, My Thoi hamlet, My Xuong commune, Cao Lanh district, Dong Thap province, and then RHA was pretreated and dried. The amount of SiO_2 in RHA was 96.7%, which was determined by the XRF measurement. Next, 10 g of RHA (containing 9.67 g of SiO_2) was boiled in reflux with 4 M NaOH for 4 h at 90ºC, then collect the solution and precipitate again with HCl solution, filtered the precipitate and washed it several times with distilled water until neutral pH, then dried at 100ºC for 72 h to obtain pure SiO_2.

In this study, a simple one-pot method to cover ferromagnetic cores with SiO_2 was proposed. First, 0.54 g of $FeCl_3.6H_2O$ was dissolved in 2wt% PVP10 and stirred for 1 h and 40 min. at 90ºC, the temperature was then lowered to 80ºC for 20 min., 0.5 M $NaBH_4$ was quickly added into the resulting solution for 15 min. The color of the solution changed from orange to black immediately afterward. Next, 0.25 g of SiO_2 was added to the above reaction mixture with a controlled pH of 12 using 25% NH_4OH solution. The mixture was maintained for 1 h and 40 min. at the above temperature, then cooled to room temperature, magnetically separated by a magnet, and then washed many times with distilled water and ethanol.

The product was dried at 60°C under pressure of 0.5 atm for 6 h (Thanh et al., 2020).

2.2.2. Synthesis of Fe_3O_4@zeolite NaA

In this work, Fe_3O_4@zeolite NaA was synthesized using the hydrothermal method. To this end, 0.5 g Fe_3O_4@SiO_2 containing 0.4264 g SiO_2 determined by inductively coupled plasma atomic emission spectroscopy measurement (85.27% SiO_2 and 14.72% Fe_3O_4) was first dispersed into 4 M NaOH by ultra-sonication for 15 min. In the meantime, 0.83 g $NaAlO_2$ was dissolved in 10 mL of distilled water. After that, this solution was added to the above mixture (Si/Al=1.4) and continued to ultrasonic for 15 min., then the mixture was placed into Teflon lined hydrothermal autoclave at 110ºC to crystallize for 10 h. After that, the above suspension was magnetically sedimented and was several times with distilled water until pH 7.0. Finally, the sample was dried at 60ºC for 6 h under a pressure of 0.5 atm.

2.2.3. Characterization of Fe_3O_4@SiO_2 and Fe_3O_4@zeolite NaA

To clarify the properties of the materials, Fe_3O_4@SiO_2 and Fe_3O_4@zeolite NaA were subjected to X-ray diffraction (XRD) analysis using a D8 Advance instrument (Bruker) to determine the material structure. The bonds of the synthesized materials were determined through Fourier transform infrared spectroscopy (FTIR) using a NICOLET 6700 instrument (Thermo). The morphology of the material was determined through the results of scanning electron spectroscopy combined with field emission (FE-SEM) using a JEOL-JCM 7000 device. Besides, using Nova 1000e, Quantachrome determines specific surface area, pore diameter, and pore volume. The Microsense EZ9 vibrating sample magnetometer (VSM) (Microsense) was used to determine the saturation magnetization of both Fe_3O_4@SiO_2 and Fe_3O_4@zeolite NaA. The surface charge of Fe_3O_4@zeolite NaA was measured by the salt method (Kosmulski, 2012). In addition, in this study, the inductively coupled plasma atomic emission spectroscopy (ICP-EAS) (Optima 7300 DV, PerkinElmer) was used to determine ferromagnetic content and silica in solution to calculate the Si:Al ratio for the next step. Finally, Fluorescence Spectroscopy (XRF) - (Horiba MESA-50) was used to determine the mass percentage of oxides in the RHA sample.

2.3. Adsorption experiment

The MB adsorption process was investigated at fixed conditions, using the variable-by-variable method to determine the optimal conditions for the process. The pH factor was adjusted from 4.0 to 9.0 using 0.1 M NaOH and 0.1 M HCl solution, and the adsorbent concentration varied from 10 mg/L to 40 mg/L for periods of 15 to 120 min. MB concentrations before and after adsorption were determined at λ_{max} of 665 nm by UV-Vis measurement (Labomed, UVD-3500) method after magnetic sedimentation to remove the adsorbent.

Adsorption capacity q_c (mg/g) and adsorption efficiency H (%) were calculated according to the following formula.

$$q_c = \frac{(C_o - C_c)V}{m} \quad (1)$$

$$H = \frac{(C_o - C_c)}{C_o} \times 100\% \quad (2)$$

where q_c (mg/g) is the adsorption capacity, C_0 (mg/L) and C_c (mg/L) are the MB concentration before and after adsorption, respectively, V (mL) is the solution volume, and m (g) is adsorbent mass.

2.4. Adsorption kinetics and isotherms

Pseudo-first-order (PFO) and pseudo-second-order (PSO) were ordinarily used in reaction kinetics. While PFO assumed that MB-occupied sites had a linear relationship with the rate of adsorption/desorption, stated that the square of the number of the sites filled by MB had a linear relationship with the rate of adsorption/desorption. The adsorption capacity of PFO and PSO rate expression can be expressed by Eq. (3) and (4) (Cheung et al., 2003; Kowanga et al., 2016).

$$\log(q_e\text{-}q_t) = \log q_e - \frac{K_1}{2.303}t \quad (3)$$

$$\frac{t}{q_t} = \frac{1}{k_2 \cdot q_e^2} + \frac{1}{q_e} \quad (4)$$

where, k_1 (1/min) represents the adsorption rate constant, k_1 and q_e can be obtained by plotting a fitted linear graph of $\log(q_e\text{-}q_t)$. k_2 (g/mg.min.) is a PSO rate constant, and k_2 and q_e are determined by plotting a fitted straight-line graph with t as the X-axis and t/q_t as the Y-axis.

The interaction between Fe_3O_4@zeolite NaA and MB can be described by adsorption isotherms, in which Langmuir and Freundlich models are normally used to study equilibrium data. The Langmuir model was practical for a monolayer adsorbate on the homogeneous surface of the

adsorbent without interactions between the adsorbed dye molecules. The Langmuir expression was as Eq. (5) (Kocaoba et al., 2007). On the other hand, the Freundlich model supposed that adsorption took place on the heterogeneous surface, and it was indicated by Eq. (6) (Panayotova, 2001).

$$\frac{C_e}{q_e} = \frac{1}{q_{max} K_L} + \frac{C_e}{q_{max}} \quad (5)$$

where q_e (mg/g) is the amount of adsorbate per weight of adsorbent, q_{max} (mg/g) designates maximum adsorption capacity, C_e (mg/L) is the equilibrium concentration of adsorbate, and K_L (L/mg) is Langmuir characteristic constants, which shows the adsorption energy.

$$\text{Log}q_e = \frac{1}{n}.\log C_e + \log k_F \quad (6)$$

Where K_F (L/mg) and 1/n are Freundlich characteristic constants representing adsorption capacity and adsorption intensity, respectively.

The Dubinin–Radushkevich (D–R) model is normally applied to distinguish between physical and chemical adsorption, and its linear form is given as Eq. (7) (Perié et al., 2004).

$$\ln q_e = \ln q_m - \beta.\varepsilon^2 \quad (7)$$

where q_e is the amount of the dye adsorbed per weight of adsorbent (mg/g), ε is the Polanyi potential intended from Eq. (8). The values of q_m and β can be calculated from the slope and intercept of the plot of ln q_e. The constant β provides valuable information about the mean free energy E (kJ/mol) of adsorption per molecule of adsorbate and it can be designed using Eq. (9).

$$\varepsilon = RT\ln\left(1+\frac{1}{C_e}\right) \quad (8)$$

$$E = \frac{1}{\sqrt{-2\beta}} \quad (9)$$

The value of E is respected for evaluating the types of adsorption processes. The adsorption type can be defined by physical adsorption once E < 8.0 kJ/mol (Perié et al., 2004).

3. RESULTS AND DISCUSSION

3.1. Material properties characteristics

3.1.1. XRD and FT-IR

X-ray diffraction results of Fe_3O_4@SiO_2 and Fe_3O_4@zeolite NaA were shown in Figure 1a. For Fe_3O_4@SiO_2, Figure 1a showed some of the characteristic peaks of Fe_3O_4 observed at positions 2θ = 30.5°, 35.5°, 43°, 57°, and 62.5°. This result was consistent with the standard card of Fe_3O_4 (JCPDS 19-0629). The XRD pattern of Fe_3O_4@SiO_2 not only contained the characteristic peaks of Fe_3O_4 nanoparticles but also some broader and low-intensity peaks at 2θ = 20°-30° corresponding to an amorphous SiO_2 coating layer (Cao et al., 2020). For Fe_3O_4@zeolite NaA in Figure 1a, the diffraction peaks at 2θ = 30.4°, 35.6°, 43.2° and 62.5°characterized the presence of Fe_3O_4 nanoparticles, while the peaks at positions 2θ = 7.0°, 10.3°, 22.3°, 24.2°, 29°, and 34.2° were characteristic peaks of zeolite NaA by the standard card (JCPDS 00-039-0222) proving that Fe_3O_4 @zeolite NaA was successfully synthesized. However, some new diffraction peaks appeared at positions 2θ = 14.5° and 60° due to the growth orientation of surfactants or impurities.

FT-IR spectra of SiO_2, Fe_3O_4, Fe_3O_4@SiO_2, and Fe_3O_4@zeolite NaA were presented in Figure 1b. For SiO_2, the absorption bands assigned to Si–O at 467 cm^{-1} and Si–O–Si at 1093 cm^{-1} (Liang et al., 2012), and no other significant peaks were observed; thus, it could state that the SiO_2 recovered from RHA was quite pure. Figure 1b also showed that Fe_3O_4 nanoparticles had a wavelength of 592 cm^{-1} belonging to the stretching vibration region of the Fe–O bond, this was the characteristic wavelength of Fe_3O_4 nanoparticles. In addition, there was no appearance of the characteristic 632 cm^{-1} wavelengths of Fe_2O_3, which proved the formation of single-phase Fe_3O_4 and high stability during the synthesis process. The wavelengths at positions 3425 cm^{-1} and 1633 cm^{-1} were related to –OH relaxation and deformation vibrations, respectively. These bands indicated the existence of hydroxyl groups connected to the surfaces of Fe_3O_4 nanoparticles (Karimzadeh et al., 2016).

From the FT-IR spectrum of Fe_3O_4@SiO_2 in Figure 1b, it could state that the absorption peak at 456 cm^{-1} was the bending vibration of the Si–O bond and also presented in the FT-IR spectrum of Fe_3O_4@zeolite NaA, which was related to the internal bond vibrations of the TO_4 tetrahedron (T = Si or Al) in the zeolite structure. The absorption peaks at 589 and 1017 cm^{-1} corresponded to the bending vibration of Fe–O and the stretching vibration of Si–OH, while the vibration at 717cm^{-1} characterized the stretching vibration of the bond Si-O-Al (Jiang et al., 2016). Finally, in the spectrum of Fe_3O_4@zeolite NaA, the wavelength at position 656 cm^{-1} was commonly known as the vibration of the Si-O-M bond (M is the metal ion), and in this study,

M could be the Na^+ ion, which was exchanged (Nibou et al., 2009). In summary, the presence of Si-O-Al and Si-O-Na bonds demonstrated that zeolite NaA had been successfully crystallized with a ferromagnetic nanoparticle core.

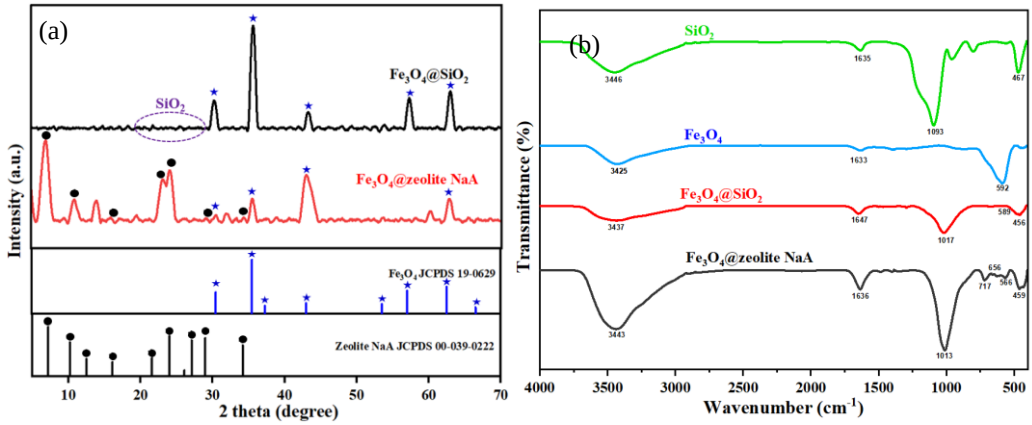

Figure 1. (a) XRD of Fe_3O_4@SiO_2, Fe_3O_4@zeolite NaA, and (b) FT-IR spectra of SiO_2, Fe_3O_4, Fe_3O_4@SiO_2 and Fe_3O_4@zeolite NaA

3.1.2. FE-SEM and BET

FE-SEM images of Fe_3O_4@SiO_2, and Fe_3O_4@zeolite NaA were used to evaluate surface morphology, and the results were presented in Figure 2. Results in Figure 2a showed that nano-sized Fe_3O_4@SiO_2 had been formed, but there was a phenomenon of clumping together. The results in Figure 2b showed that Fe_3O_4@zeolite NaA was formed with a fairly uniform size. The particle size distribution in Figure 2c determined the average size of Fe_3O_4@zeolite NaA to be 0.981±0.235 µm via ImageJ2 software. In addition, Fe_3O_4@zeolite NaA had a relatively cubic and spherical structure, and this result was quite similar to the previous report (Cao et al., 2020).

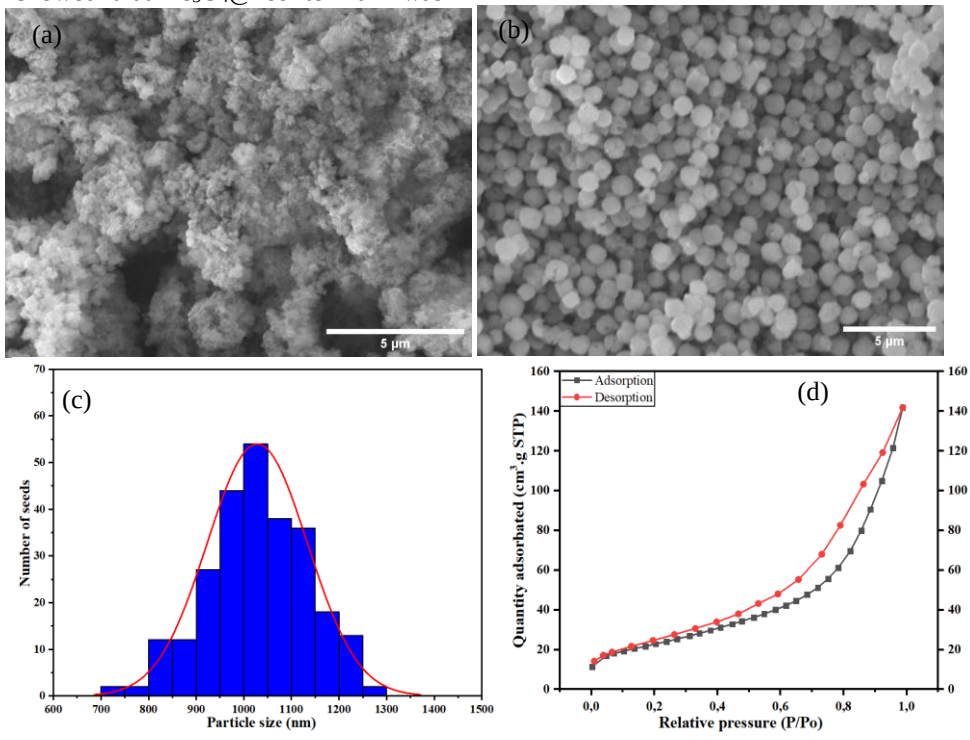

Figure 2. FE-SEM of (a) Fe_3O_4@SiO_2, (b) Fe_3O_4@zeolite NaA, (c) size distribution of Fe_3O_4@zeolite NaA and (d) Nitrogen adsorption-desorption isotherm of Fe_3O_4@zeolite NaA

The specific surface area of the material is determined by the adsorption isotherm according to the BET (Brunauer-Emmett-Teller) method. The surface area of Fe_3O_4@zeolite NaA was determined to be 82.4 m^2/g, which was larger than the surface area (31.6 m^2/g) of zeolite NaA synthesized from RHA by single-step process (Kumar & Naskar, 2019). The pore volume and the pore diameter of Fe_3O_4@zeolite NaA are 0.224 cm^3/g and 1.019 nm, respectively. The above results demonstrated that Fe_3O_4@zeolite NaA was a microporous structure and Figure 2d also indicated that the N_2 adsorption-desorption of Fe_3O_4@zeolite NaA was listed as type IV isotherm representing a monolayer-multilayer adsorption that could be happened in porous structure (Sing, 1985; ALOthman, 2012). These findings suggested that Fe_3O_4@zeolite NaA had good adsorption capacity for MB^+ possessing a diameter of 0.95 nm (Jia et al., 2018).

3.1.3. *VSM and surface charge of Fe_3O_4@zeolite NaA*

VSM results in Figure 3a showed the hysteresis cycle of Fe_3O_4@SiO_2 and Fe_3O_4@zeolite NaA at room temperature. Both showed good magnetization curves after being coated with SiO_2 and further crystallized to form zeolite NaA, with almost zero remanence and low coercivity, proving that these particles had superparamagnetic properties. This superparamagnetic property allowed the particles to respond to an applied magnetic field, without any permanent magnetization, and to disperse rapidly when the magnetic field was lost. The magnetization of Fe_3O_4@SiO_2 was 21.79 emu/g. Besides, the decrease in magnetization of the material Fe_3O_4@zeolite NaA to 17.65 emu/g was due to the crystallization process of SiO_2 covering the outside of the ferromagnetic iron to form zeolite NaA, making the coating outside the iron core. The magnet became thicker, thereby reducing the magnetization of the material. However, Fe_3O_4@zeolite NaA still could be separated easily by magnets.

The surface charge of particles was evaluated, and the results obtained in Figure 3b showed the change in surface charge of Fe_3O_4@zeolite NaA from positive to negative with increasing pH. Figure 4b showed that the isoelectric point of Fe_3O_4@zeolite NaA was 7.48. The material surface was positively charged when pH < 7.48 and negatively charged when pH > 7.48. It can be predicted that at pH < 7.48 the material was good at adsorbing anions, and at pH > 7.48, the material could be good at adsorbing cations (MB^+), so it can be predicted that MB^+ was likely to be adsorbed by the surface of Fe_3O_4@zeolite NaA when pH > 7.48.

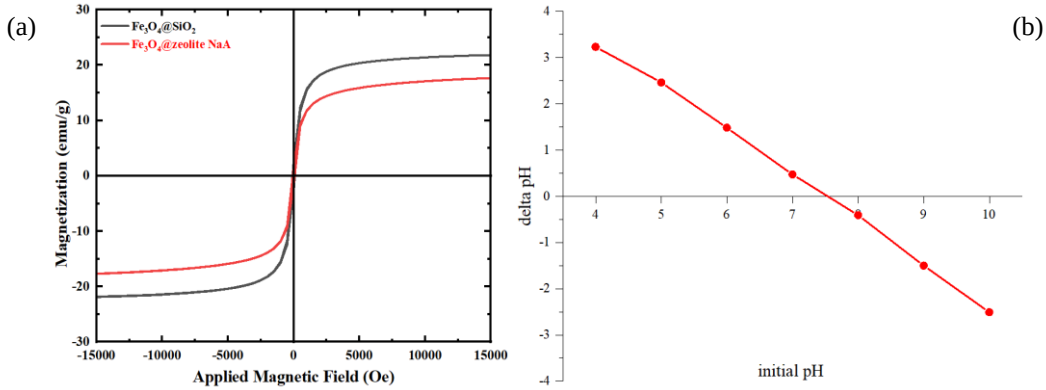

Figure 3. (a) Magnetization curves of Fe_3O_4@SiO_2 and Fe_3O_4@zeolite NaA, and (b) surface charge of Fe_3O_4@zeolite NaA material as a function of initial pH

3.2. Adsorption of MB using Fe_3O_4 @zeolite NaA

3.2.1. *Effect of pH, contact time, initial concentration, and adsorbent mass*

The adsorption of MB in water was studied at fixed conditions, using the variable-by-variable method to determine the optimal conditions for the process. In this work, four variables, such as pH, contact time, initial concentration, and adsorbent mass, were surveyed.

In an aqueous solution, MB was basically dissociated to be cationic ions (MB^+). When at pH > 7.48, the negative charge on the surface of Fe_3O_4@zeolite NaA was favorable for MB^+ adsorption. Specifically, as pH gradually increased

from 4.0 to 9.0, the adsorption efficiency increased as in Figure 4a. At pH 4.0, Fe_3O_4@zeolite NaA showed fairly low adsorption with the efficiency of 51.8±2.6%. At pH 6.0, MB adsorption efficiency progressively increased to 69.3±2.1%, and then rocketed to 79.4±2.1% at pH 8.0 and slightly rose to 82.3±1.1% when pH was 9.0. The rapid rise in MB adsorption efficiency using Fe_3O_4@zeolite NaA was mainly attributed to the shift of surface charge of the adsorbent at pH_{pzc} 7.48. Therefore, the main force that kept MB^+ adsorbed onto the negatively charged surface of the adsorbent was electrostatic interaction.

The study on the effect of MB adsorption capacity over time presented in Figure 4b showed that the MB adsorption rate of Fe_3O_4@zeolite NaA increased rapidly until reaching the highest yield of 85.6±1.6% at 25 min. and slightly decreased by about 1.5% after that. It could be that adsorbent was in fine powder form so it was easy to disperse into a solution and with a porous structure, the contact area was large so the adsorption process took place quickly at the initial contact time. Likewise, the active sites in the pores of the adsorbent were vacant, so MB^+ was swiftly adsorbed, causing a speedy increase in adsorption yield within the first 25 min. After 25 min., the adsorption yield showed a minor decrease and remained almost unchanged until 120 min., which was proven that an appropriate time was needed for the adsorbent and adsorbate to come into contact and for the adsorption process to occur completely. This result was also in good agreement with the adsorption of organic colorants by using rice husk (Rehman et al., 2011). Therefore, a 25-minute contact time was chosen to further investigate.

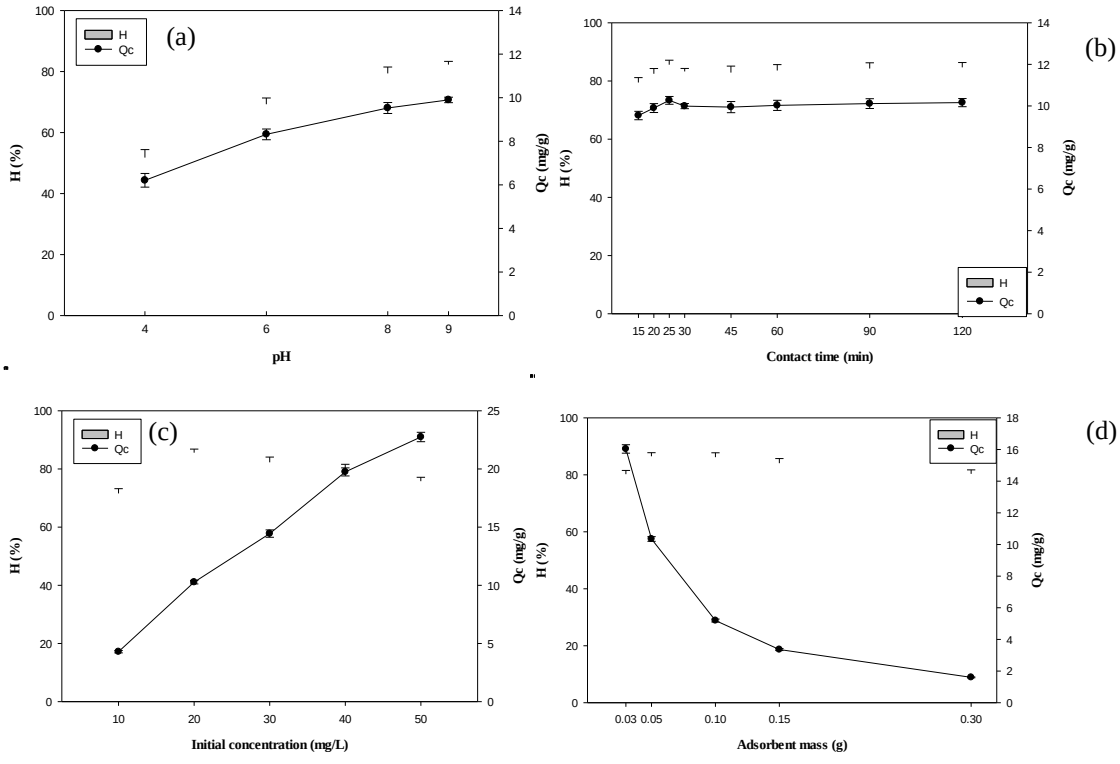

Figure 4. Effect of (a) pH, (b) effect of contact time, (c) effect of initial concentration, and (d) effect of Fe_3O_4@zeolite NaA mass on MB adsorption ability

MB concentration was initially surveyed in levels of 10, 20, 30, 40, and 50 mg/L. Figure 4c showed that as concentration increased from 10 to 20 mg/L, adsorption efficiency rose rapidly from 71.6±1.6% to 85.6±1.2%; at the same time, adsorption capacity increased from 4.29±0.11 mg/g to 10.27±1.15 mg/g. This could be that when MB concentration increased, mass transfer kinetics were higher, leading to enhanced MB diffusion from the bulk solution to the surface of the adsorbent, which

caused an increase of MB adsorption yield in a concentration ranging from 10 mg/L to 20 mg/L (Yang et al., 2011). The adsorption efficiency, however, decreased gradually from 85.6±1.2% to 75.8±1.3% due to the limit of active sites on adsorbent versus a significant number of MB^+ as its concentration varied from 20 mg/L to 50 mg/L (Mohammed et al., 2016). In other words, the low-concentration solution had fewer dye molecules than the high-concentration solution, leading to a small concentration gradient, making the diffusion of MB molecules into the adsorbent slower than in high-concentration solutions. However, since dye molecule content was low, the adsorption efficiency of dilute solutions was higher than that of the high concentration solutions. Meanwhile, adsorption capacity increased continuously from 10.27±0.15 to 22.75±0.41 mg/g, this was attributed to the fact that, when increasing MB concentration, it was more dyes adsorbed onto the adsorbent surface, while the amount of adsorbent kept unchanged, causing an increase in adsorption capacity. Finally, MB initial concentration at 20 mg/L was used to study the effect of subsequent factors in this study.

The influence of Fe_3O_4@zeolite NaA mass on MB adsorption was investigated using different amounts of adsorbent ranging from 0.03 to 0.30 g as in Figure 4d. The results showed that adsorption efficiency increased from 80.2±1.3% to 86.5±1.2% as mass varied from 0.03 g to 0.05 g, but the adsorption capacity gradually decreased with increasing mass values. When adsorbent mass rose from 0.05 g to 0.3 g, adsorption efficiency decreased from 86.5±1.2% to 80.3±1.4%. This could be because the number of adsorption centers increased as intensifying adsorbent dose, causing an increase in adsorption efficiency. However, due to the fine powder form of Fe_3O_4@zeolite NaA, when the mass increased at the identical solution volume conditions, the material tended to agglomerate, reducing the adsorption surface area or shielding and preventing MB from coming into contact with the material surface, thereby lowering the adsorption efficiency but not significantly (Ghoroi et al., 2013). Through the above results, Fe_3O_4@zeolite NaA dose used to adsorb MB was selected to be 0.05 g so that the adsorption process was stable and avoided wasting the adsorbent.

3.2.2. Adsorption kinetics and isotherms

The computed parameters of PFO and PSO equation of MB adsorption using Fe_3O_4@zeolite NaA are presented in Table 1. The results showed that R^2 of the PFO equation was 0.918 and q_e = 0.365 mg/g was lower than the experimental one indicating that MB adsorption process was not appropriate to PFO kinetics. Meanwhile, R^2 of PSO equation was high (R^2 = 0.999), and its q_e (q_e = 13.77 mg/g) was also higher than the experimental q_e. This presented that the MB adsorption obeyed PSO adsorption kinetics.

It is notable that the slope coefficient is small, producing a great adsorption capacity. In other words, when the slope coefficient is small, t/q_t will be small. Since q_t is inversely proportional to t/q_t, a small slope coefficient will increase the MB processing speed of the material. Therefore, determining the kinetic equations is important in this process. From there, predict whether the MB adsorption capacity of the materials is fast or slow. Regarding the slope coefficient of the PSO equation, a = 0.104 was relatively low, showing that the adsorption ability of Fe_3O_4@zeolite NaA to MB was quite high.

Table 1. The calculated parameters of PFO and PSO for adsorbing MB using Fe_3O_4@zeolite NaA

Parameters	PFO	PSO
a	0.004	0.104
b	-1.008	-0.073
q_e (mg/g)	0.365	13.77
k_1 (1/min.)	-0.033	-
k_2 (g/mg.min.)	-	0.051
R^2	0.918	0.999

With the results obtained from the effect of initial MB concentration, the adsorption equilibrium study was conducted according to the Langmuir and Freundlich isotherm model. The results of the adsorption isotherm parameters according to the above two models are presented in Table 2. Freundlich isotherm model had a linear regression coefficient (R^2 = 0.982) higher than that of Langmuir (R^2 = 0.948). According to Langmuir model, with K_L = 0.018 L/mg, it was in the range $0 < K < 1$, which was a meaningful adsorption process that was favorable and reversible (Hydari et al., 2012). For Freundlich model, when n = 0.678 or 1/n = 1.475, the adsorption is quite good due to the system number and the angle of the line being low. The high linear regression showed that the MB adsorption by Fe_3O_4@zeolite NaA obeyed Freundlich isotherm, verifying that the adsorption process was reversible, adsorption energy on the surface was not uniform, and the adsorbent could adsorb multilayers (López-Luna et al., 2019).

Table 2. Parameters of the Langmuir and Freundlich adsorption isotherm model

Parameters	Langmuir isotherm	Freundlich isotherm
q_{max} (mg/g)	47.66	-
n	-	0.678
K_L (L/mg)	0.018	-
K_F (L/mg)	-	1.021
R^2	0.948	0.982

The Dubinin–Radushkevich isotherm model was also applied to determine whether the adsorption mechanism was chemical or physical. Besides, it is applied to predict two important parameters adsorption capacity and free energy of adsorption (Atar et al., 2012). The results of the dependence of lnq_e on β^2 in D–R equation determined the isothermal constants. The adsorption energy constant was determined to be 1.383 kJ/mol, showing a weak interaction between MB and Fe_3O_4@zeolite NaA, or in other words, physical adsorption was the main adsorption mechanism in this study.

3.2.3. Reusability

To increase the applicability of Fe_3O_4@zeolite NaA in practical dye treatment, the reusability of material was presented in Figure 5. Experimental results showed MB removal efficiency decreased from 86.7±1.3% to 48.6±2.3% in 4 cycles. In general, the first two cycles showed that adsorption efficiency had a little change from 86.7±1.3% to 79.8±1.2%. However, starting from the 3rd and 4th cycles, the efficiency decreased sharply to 53.1±1.8% and 48.6±2.3%, respectively. It showed that starting from the 3rd cycle, the adsorption activity of the adsorbent gradually vanished, which could be due to the occupancy of adsorption sites by MB (Vidovix et al., 2022). It is concluded that the Fe_3O_4@zeolite NaA had good adsorption capacity in 2 cycles.

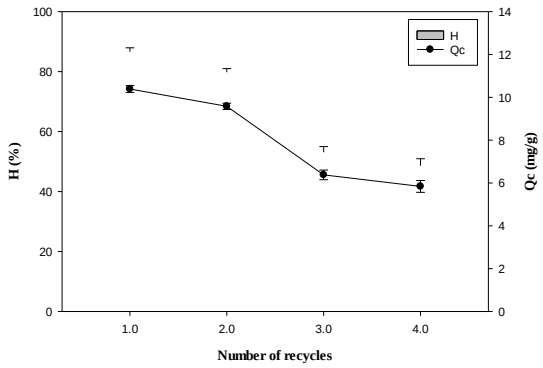

Figure 5. Reuse of Fe_3O_4@zeolite NaA for adsorbing MB

Compared to other materials, Fe_3O_4@zeolite NaA shows a high adsorption capacity (Table 3). Indeed, MB adsorption capacity of ZSM-5 was 8.67 mg/g (Jin et al., 2008), while zeolite and zeolite NaY showed a higher adsorption capacity of 22 and 31.41 mg/g, respectively (Rida er al., 2013; EL-Mekkawi et al., 2016). The adsorption capacity of MB was improved to be 40.36 mg/g when using Fe_3O_4/ZA. However, this value was lower than the MB adsorption capacity (47.66 mg/g) in this work due to its low specific surface area.

Table 3. MB adsorption performance in comparison with other studies

Adsorbents	MB adsorption capacity (mg/g)	References
Zeolite (ZSM-5)	8.67	Jin et al., 2008
Zeolite (ECC International)	22	Rida et al., 2013
Zeolite NaY	21.41	EL-Mekkawi et al., 2016
Fe_3O_4/ZA	40.36	Tran et al., 2021
Fe_3O_4@zeolite NaA	47.66	This work

4. CONCLUSION

Fe_3O_4@zeolite NaA was successfully synthesized by combining ferromagnetic particles with zeolite NaA through the intermediate precursor Fe_3O_4@SiO_2 developed by coating with SiO_2 recovered from RHA. Fe_3O_4@zeolite NaA had an average particle size of 0.98±0.23 μm with a cubic shape, a large surface area of 82.41 m^2/g, a pore diameter of 1.019 nm, and a pore volume of 0.224 cm^3/g, which was suitable for the adsorption of organic dye MB. Fe_3O_4@zeolite NaA had a magnetization of 17.65 emu/g with a good ability to magnetically settle and separate from the solution after adsorption. The adsorbent applied to MB adsorption achieved the highest adsorption efficiency of 86.5% at room temperature with an initial MB concentration of 20 mg/L, pH 9 for 25 min., and adsorbent mass of 0.05 g. MB adsorption onto Fe_3O_4@zeolite NaA was a physical interaction and in good agreement with Freundlich isotherm and PSO. The adsorbent could also be reused for two to three times. The above results indicated that

Fe_3O_4@zeolite NaA material had the potential to adsorb dyes on an industrial scale.

ACKNOWLEDGMENTS

This study is funded in part by the Can Tho University Code: T2023-118.

REFERENCES

ALOthman, Z. A. (2012). A review: fundamental aspects of silicate mesoporous materials. *Materials*, *5*, 2874-2902. https://doi.org/10.3390/ma5122874

Atar, N., Olgun, A., & Wang, S. (2012). Adsorption of cadmium (II) and zinc (II) on boron enrichment process waste in aqueous solutions: batch and fixed-bed system studies. *Chemical Engineering Journal*, *192*(1), 1-7. https://doi.org/10.1016/j.cej.2012.03.067

Cao, J., Wang, P., Shen, J., & Sun, Q. (2020). Core-shell Fe_3O_4@zeolite NaA as an Adsorbent for Cu^{2+}. *Materials*, *13*(21), 5047. https://doi.org/10.3390/ma13215047

Chandrakant, R. H., Ananda, J. J., Dipak, V. P., Naresh, M. M., & Aniruddha, B. P. (2016). A critical review on textile wastewater treatments: Possible approaches. *Journal of Environmental Management*, *182*, 351-366. https://doi.org/10.1016/j.jenvman.2016.07.090

Cheung, W. H., Ng, J. C. Y., & Mckey, G. (2003). Kinetic analysis of the sorption of copper(II) ions on chitosan. *Journal of Chemical Technology and Biotechnology*, *78*, 562-571. https://doi.org/10.1002/jctb.836

EL-Mekkawi, D. M., Ibrahim, F. A., & Selim, M. M. (2016). Removal of methylene blue from water using zeolites prepared from Egyptian kaolins collected from different sources. *Journal of Environmental Chemical Engineering*, *4*, 1417-1422. https://doi.org/10.1016/j.jece.2016.01.007

Galán, J., Rodríguez, A., Gómez, J. M., Allen, S. J., & Walker, G. M. (2013). Reactive dye adsorption onto a novel mesoporous carbon. *Chemical Engineering Journal*, *219*, 62-68. https://doi.org/10.1016/j.cej.2012.12.073

Ghoroi, C., Han, X., To, D., Jallo, L., Gurumurthy, L., & Davé, R. N. (2013). Dispersion of fine and ultrafine powders through surface modification and rapid expansion. *Chemical Engineering Science*, *85*, 11-24. https://doi.org/10.1016/j.ces.2012.02.038

Hydari, S., Sharififard, H., Nabavinia, M., & Parvizi, M. R. (2012). A comparative investigation on removal performances of commercial activated carbon, chitosan biosorbent and chitosan/activated carbon composite for cadmium. *Chemical Engineering Journal*, *193-194*, 276-282. https://doi.org/10.1016/j.cej.2012.04.057

Jia, P., Tan, H., Liu, K., & Gao, W. (2018). Removal of methylene blue from aqueous solution by bone char. *Applied Science*, *8*, 1903. https://doi.org/10.3390/app8101903

Jiang, Z., Yang, J., Ma, H., Ma, X., & Yuan, J. (2016). Synthesis of pure NaA zeolites from coal fly ashes for ammonium removal from aqueous solutions. *Clean Technologies and Environmental Policy*, *18*, 629-637. https://doi.org/10.1007/s10098-015-1072-0

Jin, X., Jiang, X. Q., Shan, X. Q., Pei, Z. G., & Chen, Z. (2008). Adsorption of methylene blue and orange II onto unmodified and surfactant-modified zeolite. *Journal of Colloid and Interface Science*, *328*, 243-247. https://doi.org/10.1016/j.jcis.2008.08.066

Karimzadeh, I., Aghazadeh, M., Ganjali, M. R., Norouzi, P., Shirvani-Arani, S., Doroudi, T., Kolivand, P. H., Marashi, S. A., & Gharailou, D. (2016). A novel method for preparation of bare and poly (vinylpyrrolidone) coated superparamagnetic iron oxide nanoparticles for biomedical applications. *Materials Letters*, *179*, 5-8. https://doi.org/10.1016/j.matlet.2016.05.048

Khaleque, A., Alam, M. M., Hoque, M., Mondal, S., Haider, J. B., Xu, B., Johir, M. A. H., Karmakar, A. K., Zhou, J. L., Ahmed, M. B., & Moni, M. A. (2020). Zeolite synthesis from low-cost materials and environmental applications: A review. *Environmental Advances*, *2*, 100019. https://doi.org/10.1016/j.envadv.2020.100019

Kocaoba, S., Orhan, Y., & Akyüz, T. (2007). Kinetics and equilibrium studies of heavy metal ions removal by use of natural zeolite. *Desalination*, *214*, 1-10. https://doi.org/10.1016/j.desal.2006.09.023

Kosmulski, M. (2012). IEP as a parameter characterizing the pH-dependent surface charging of materials other than metal oxides. *Advances in Colloid and Interface Science*, *171-172*, 77-86. https://doi.org/10.1016/j.cis.2012.01.005

Kowanga, K. D., Gatebe, E., Mauti, G. O., & Mauti, E. M. (2016). Correspondence: Kinetic, sorption isotherms, pseudo-first-order model and pseudo-second-order model studies of Cu(II) and Pb(II) using defatted Moringa oleifera seed powder. *The Journal of Phytopharmacology*, *5*, 71-78. https://doi.org/10.31254/phyto.2016.5206

Kumar, A., & Naskar, M. K. (2019). Single-step process without organic template for the formation of zeolite A from RHA. *International Journal of Applied Ceramic Technology*, *16*(4), 1525-1532. https://doi.org/10.1111/ijac.13206

Liang, Y., Ouyang, J., Wang, H., Wang, W., Chui, P., & Sun, K. (2012). Synthesis and characterization of core–shell structured SiO_2@YVO_4:Yb^{3+}, Er^{3+}

microspheres. *Applied Surface Science*, *258*, 3689-3694. https://doi.org/10.1016/j.apsusc.2011.12.006

Liu, H., Peng, S., Shu, L., Chen, T., Bao, T., & Frost, R. L. (2013a). Effect of Fe_3O_4 addition on removal of Zeolite NaA-ammonium complex. *Journal of Colloid and Interface Science*, *390*(1), 204-210. https://doi.org/10.1016/j.jcis.2012.09.010

Liu, H., Peng, S., Shu, L., Chen, T., Bao, T., & Frost, R. L. (2013b). Magnetic zeolite NaA: Synthesis, characterization based on metakaolin and its application for the removal of Cu^{2+}, Pb^{2+}. *Chemosphere*, *91*(11), 1539-1546. https://doi.org/10.1016/j.chemosphere.2012.12.038

López-Luna, J., Ramírez-Montes, L. E., Martinez-Vargas, S., Martínez, A. I., Mijangos-Ricardez, O. F., González-Chávez, M. d. C. A., Carrillo-González, R., Solís-Domínguez, F. A., Cuevas-Díaz, M. d. C., & Vázquez-Hipólito, V. (2019). Linear and nonlinear kinetic and isotherm adsorption models for arsenic removal by manganese ferrite nanoparticles. *SN Applied Science*, *1*, 950. https://doi.org/10.1007/s42452-019-0977-3

Mai, N. T. N., Thu, N. T. A., Trang, N. T. B., Phu, P. Q., Thien, D. V. H., Thanh, L. H. V., & Hanh, C. L. N. (2021). Adsorption of chromium (VI) ion using zeolite NaA/Fe_3O_4 composite derived from rice husk ash. *In IOP Conference Series: Earth and Environmental Science*, *947*(1), 012012. https://doi.org/10.1088/1755-1315/947/1/012012

Mohammed, N., Grishkewich, N., Waeijen, H. A., Berry, R. M., & Tam, K. C. (2016). Continuous flow adsorption of methylene blue by cellulose nanocrystal-alginate hydrogel beads in fixed bed columns. *Carbohydrate Polymers*, *136*, 1194-1202. https://doi.org/10.1016/j.carbpol.2015.09.099

Nibou, D., Amokrane, S., Mekatel, H., & Lebaili, N. (2009). Elaboration and characterization of solid materials of types zeolite NaA and faujasite NaY exchanged by zinc metallic ions Zn^{2+}. *Physics Procedia*, *2*(3), 1433-1440. https://doi.org/10.1016/j.phpro.2009.11.113

Oladoye, P. O. (2022). Natural, low-cost adsorbents for toxic Pb(II) ion sequestration from (waste)water: A state-of-the-art review. *Chemosphere*, *287*, 132130. https://doi.org/10.1016/j.chemosphere.2021.132130

Panayotova, M. I. (2001). Kinetics and thermodynamics of copper ions removal from wastewater by use of zeolite. *Waste Management*, *21*(7), 671-676. https://doi.org/10.1016/S0956-053X(00)00115-X

Perić, J., Trgo, M., & Medvidović, N. V. (2004). Removal of zinc, copper and lead by natural zeolite—a comparison of adsorption isotherms. *Water Research*, *38*(7), 1893-1899. https://doi.org/10.1016/j.watres.2003.12.035

Rehman, R., Anwar, J., Mahmud, T., Salman, M., Shafique, U., & Zaman, W. U. (2011). Removal of murexide (dye) from aqueous media using rice husk as an adsorbent. *Journal of the Chemical Society of Pakistan*, *33*(4), 598-603

Rida, K., Bouraoui, S., & Hadnine, S. (2013). Adsorption of methylene blue from aqueous solution by kaolin and zeolite. *Applied Clay Science*, *83-84*, 99-105. https://doi.org/10.1016/j.clay.2013.08.015

Sing, K. S. W. (1985). Reporting physisorption data for gas/solid systems with special reference to the determination of surface area and porosity. *Pure Applied Chemistry*, *57*, 603-619. https://doi.org/10.1351/pac198557040603

Thanh, L. H. V., Lan, T. N. P., Quyen, T. T. B., Nam, H. Q., & Tho, L. P. B. (2020). Adsorption behavior of Cr(VI) ion on Fe_3O_4@SiO_2 with SiO_2 originated from rice husk ash. *Can Tho University Journal of Science*, *56*(3), 9-19. https://doi.org/10.22144/ctu.jvn.2020.048

Tran, N. B. T., Duong, N. B., & Le, N. L. (2021). Synthesis and characterization of magnetic Fe_3O_4/zeolite NaA nanocomposite for the adsorption removal of methylene blue potential in wastewater treatment. *Journal of Chemistry*, *2021*, 1-14. https://doi.org/10.1155/2021/6678588

Velarde, L., Nabavi, M. S., Escalera, E., Antti, M. L., & Akhtar, F. (2023). Adsorption of heavy metals on natural zeolites: A review. *Chemosphere*, *328*, 138508. https://doi.org/10.1016/j.chemosphere.2023.138508

Vidovix, T. B., Quesada, H. B., Bergamasco, R., Vieira, M. F., & Vieira, A. M. S. (2022). Adsorption of Safranin-O dye by copper oxide nanoparticles synthesized from Punica granatum leaf extract. *Environmental Technology*, *43*(20), 3047-3063. https://doi.org/10.1080/09593330.2021.1914180

Yang, S. T., Chen, S., Chang, Y., Cao, A., Liu, Y., & Wang, H. (2011). Removal of methylene blue from aqueous solution using graphene oxide. *Journal of Colloid and Interface Science*, *359*(1), 24-29. https://doi.org/10.1016/j.jcis.2011.02.064

Yusof, A. M., Nizam, N. A., & Rashid, N. A. A. (2010). Hydrothermal conversion of rice husk ash to faujasite-types and NaA-type of zeolites. *Journal of Porous Materials*, *17*, 39-47. https://doi.org/10.1007/s10934-009-9262-y

Zhang, X., Tang, D., & Jiang, G. (2013). Synthesis of zeolite NaA at room temperature: The effect of synthesis parameters on crystal size and its size distribution. *Advanced Powder Technology*, *24*(3), 689-696. https://doi.org/10.1016/j.apt.2012.12.010